Inorganic Chemistry

Article

pubs.acs.org/IC

Two New Barium Borate Fluorides $ABa_{12}(BO_3)_7F_4$ (A = Li and Na)

Jing Zhao and R. K. Li*

Beijing Center for Crystal Research and Development, Key Laboratory of Functional Crystals and Laser Technology, Technical Institute of Physics and Chemistry, Chinese Academy of Sciences, 29 Zhongguancun East Road, Beijing 100190, China

Supporting Information

ABSTRACT: Two new barium borate fluorides $LiBa_{12}(BO_3)_7F_4$ and $NaBa_{12}(BO_3)_7F_4$ are obtained by spontaneous crystallization from high-temperature flux. The two compounds are isostructural and crystallized into the tetragonal system, *I*4/*mcm* space group, with unit cell parameters of a = 13.5709(6) Å, c = 14.9908(13) Å for $LiBa_{12}(BO_3)_7F_4$ and a = 13.6443(9) Å, c = 15.021(2) Å for $NaBa_{12}(BO_3)_7F_4$. Isolated Li/NaF_4−BO_3 units formed by Li/NaF_4O square pyramids and $B3O_3$ groups sharing the O5 atom are found occupying the octagonal tunnels built by Ba and BO_3 groups along the c axis. High mobility of Li^+ ion is observed in the $LiBa_{12}(BO_3)_7F_4$ single crystal by ac impedance measurements at different temperatures.

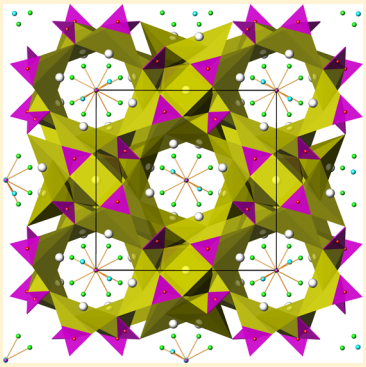

INTRODUCTION

Borate fluorides are of current interest because of their rich structural chemistry and diverse applications as catalysis, ion exchange, and nonlinear optical (NLO) materials.[1−3] Borates have extraordinary structure diversities because the boron atom can display two distinct bonding environments of triangular planar and tetrahedral coordination with oxygen. These two basic building blocks can be connected by means of corner- or edge-sharing oxygen atoms[4] to form infinite varieties of chains, sheets, or three-dimensional frameworks.[5] Among a dozen alkali and alkaline-earth metal borate fluorides the one that attracts the most attention is the deep UV nonlinear optical material $KBe_2BO_3F_2$,[6] which is transparent from 147 to 3660 nm and can generate deep ultraviolet (177.3 nm) laser output from sixth-harmonic generation of Nd:YAG lasers. Other borate fluorides including $BaCaBO_3F$, $BaZnBO_3F$, $BaAlBO_3F_2$, $M_5(BO_3)_3F$ (M = Mg, Ca), $M_3B_6O_{11}F_2$ (M = Sr, Ba), and $NaBe_2BO_3F_2$ are noncentrosymmetric and were proposed as nonlinear optical materials.[7−12]

Recently, some new borate fluorides have been discovered in the process of exploring proper flux for growth of β-BaB_2O_4 crystal, including $Ba_2Na_3[B_3O_6]_2F$, $Ba_{4-x}Sr_{3+x}(BO_3)_{4-y}F_{2+3y}$, $Ba_5(B_2O_5)_2F_2$, $Ba_7(BO_3)_{4-x}F_{2+3x}$, and $Ba_4B_{11}O_{20}F$.[13−17] In an attempt to further explore the Ba−B_2O_3−AF system, we found two novel alkaline and alkaline-earth metal fluoride borates $LiBa_{12}(BO_3)_7F_4$ and $NaBa_{12}(BO_3)_7F_4$. Both of the two compounds crystallize in a tetragonal cell with an apatite-type tunnel extending along the c axis. Alkaline fluorides in the form of AF_4 are found occupying those tunnels alternatively with isolated BO_3 groups. Similar alkaline halide salt inclusion compounds can be found in some recent reports, e.g., $[BaCl][CuPO_4]$, $Cs_2Cu_7(P_2O_7)_4{\cdot}6CsCl$, $Cs_2Cu_5(P_2O_7)_3{\cdot}3CsCl$, $Ba_4Ga_2B_8O_{18}Cl_2{\cdot}NaCl$, $[Na_3F][SnSi_3O_9]$, and $Li_3Ca_9(BO_3)_7{\cdot}2[LiF]$.[18−22] The relatively weak bonded inclusion entity LiF_4−BO_3 in the tunnel also inspired us to characterize its electrochemical properties.

EXPERIMENTAL ASPECTS

Raw materials (analytically pure) were weighed according to the molar ratio of $BaCO_3$:BaF_2:H_3BO_3:Li_2CO_3 = 3:3:3:1 for $LiBa_{12}(BO_3)_7F_4$ and $BaCO_3$:BaF_2:H_3BO_3:NaF = 3:3:3:1 for $NaBa_{12}(BO_3)_7F_4$. Starting chemicals were ground, mixed thoroughly, put into a platinum crucible, and heated to 970 °C with a heating rate of 100 °C/h. The high-temperature solution was held for 12 h at 970 °C. Afterward, the temperature was lowered to the saturation temperature around 920 and 910 °C for the Na- and Li-containing melts, respectively, and then reduced at a rate of 10 °C/day to maintain crystal growth. After the solution solidified, the furnace was cooled down to room temperature in 24 h. Crystals were separated from the flux physically. Larger $LiBa_{12}(BO_3)_7F_4$ crystals with size up to 20 × 30 × 30 mm^3 were obtained by subsequent top-seeded solution growth with seeds obtained from the previous spontaneous crystallization. The same flux and same heating procedure as the spontaneous crystallization were employed except that the cooling rate from the saturation temperature was lowered to 0.2 °C/day till the crystal reached a certain size. Then the crystal was pulled out of the flux and cooled to room temperature in 2 days.

The $LiBa_{12}(BO_3)_7F_4$ crystal with approximate dimensions of 0.11 × 0.09 × 0.05 mm^3 was selected for single-crystal X-ray diffraction data collection. Diffraction data were collected at 301 K on a Rigaku XtaLAB-mini diffractometer with a sealed tube (50 kV/12 mA) and graphite-monochromated Mo Kα radiation (λ = 0.71075 Å). Absorption and *Lp* corrections were applied with the CrystalClear program.[23] The heavy atom Ba was found by direct method with the SHELXS program,[24] and lighter atoms Li, Na, B, O, and F were found by subsequent Fourier synthesis routines. Finally, all crystallographic and atomic parameters were refined with the SHELXL program. The

Received: October 9, 2013
Published: February 20, 2014

   dx.doi.org/10.1021/ic4025525 | *Inorg. Chem.* 2014, 53, 2501−2505

structure of $NaBa_{12}(BO_3)_7F_4$ was determined in the same condition with approximate crystal dimensions of 0.09 × 0.07 × 0.05 mm^3. The final full-matrix least-squares refinement on F^2 converged to R1 = 0.0365 and wR2 = 0.0783 for $LiBa_{12}(BO_3)_7F_4$ and R1 = 0.0302 and wR2 = 0.0607 for $NaBa_{12}(BO_3)_7F_4$ from observed reflections. Crystallographic data of $LiBa_{12}(BO_3)_7F_4$ and $NaBa_{12}(BO_3)_7F_4$ are shown in Table 1.

Table 1. Crystallographic Data for $LiBa_{12}(BO_3)_7F_4$ and $NaBa_{12}(BO_3)_7F_4$

formula	$LiBa_{12}(BO_3)_7F_4$	$NaBa_{12}(BO_3)_7F_4$
space group	*I*4/*mcm*	*I*4/*mcm*
a (Å)	13.5709(6)	13.6443(9)
c (Å)	14.9908(13)	15.021(2)
V (Å^3)	2760.8(3)	2796.5(5)
Z	4	4
calcd density (g/cm^3)	5.155	5.127
cryst size (mm^3)	0.04 × 0.10 × 0.12	0.06 × 0.12 × 0.20
absorption coefficient (mm^{-1})	16.913	16.714
radiation (Mo Kα)	0.71073	0.71073
data collection range/deg	$2.122 < \theta < 27.447$	$3.438 < \theta < 27.428$
index ranges	$-17 \le h \le 17$	$-17 \le h \le 17$
	$-16 \le k \le 17$	$-17 \le k \le 17$
	$-19 \le l \le 19$	$-19 \le l \le 19$
T (K)	301	301
no. of reflns measd total	878	884
GOF	1.320	1.182
R1 (all reflns)	0.0365	0.0302
R1 ($I \ge 2\delta(I)$)	0.0346	0.0295
wR2 (all reflns)	0.0783	0.0607
wR2 ($I \ge 2\delta(I)$)	0.0764	0.0604
largest diff peak and hole (e/Å^3)	1.025, −1.098	1.151, −1.601

Single-phase powder samples of $ABa_{12}(BO_3)_7F_4$ (A = Li, Na) were synthesized in accordance with the stoichiometric ratio. Mixtures were first heated at 300 °C for 2 h and then sintered at 900 °C for 3 h with several intermediate grindings (Figure S1, Supporting Information). Variable-temperature impedance measurements were made with an Agilent 4294A Precision Impedance Analyzer in the frequency range from 40 Hz to 110 MHz with a crystal plate of 5.1 × 3.9 × 0.53 mm^3 coated with silver. Differential scanning calorimetry and thermogravimetric analysis (DSC-TG) was carried out with a NETZSCH STA449C thermal analyzer (Figure S2, Supporting Information). The optic transmission spectrum of a freshly grown $LiBa_{12}(BO_3)_7F_4$ crystal with a size of 10 × 7 × 0.5 mm^3 was recorded with a Lambda 900 UV/vis/NIR (Perkin-Elmer) spectrophotometer. A Varian 710-ES inductively coupled plasma optical emission spectrometer (ICP-OES) with SepexCertiprep standards was employed to analyze the element contents of the crystal. Raman experiments were carried out with an inVia-Reflex microzone Raman spectrometer (Figure S3, Supporting Information).

RESULTS AND DISCUSSION

Both $LiBa_{12}(BO_3)_7F_4$ and $NaBa_{12}(BO_3)_7F_4$ structures were solved with the same space group *I*4/*mcm*, and unit cell parameters are *a* = 13.5709(6) Å, *c* = 14.9908(13) Å and *a* = 13.6443(9) Å, *c* = 15.021(2) Å, respectively. In the unit cell (Figure 1), Ba atoms have three different coordination environments. Ba1 coordinated to 7 oxygen atoms with bond distances ranging from 2.52(2) to 3.049(8) Å and two F atoms with a distance of 2.823(5) and 2.916(5) Å. Ba1 atoms in the unit cell form walls of the octagonal tunnels running along the *c* axis. Such tunnel is analogous to that in the well-known apatite structure. Ba2 coordinates to six O atoms (2.618(9)−2.836(6) Å) to form a triangular prism which serves as a stitch to link the

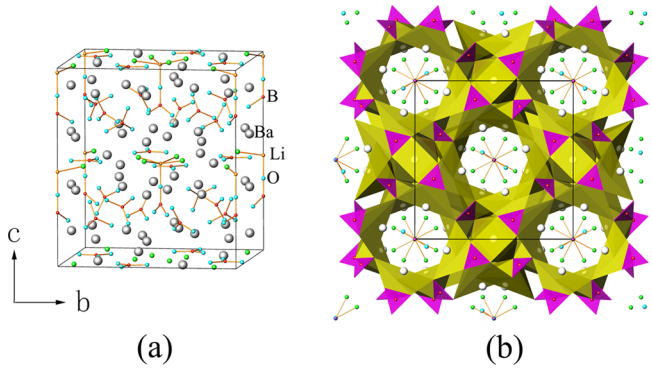

Figure 1. Unit cell contents of $LiBa_{12}(BO_3)_7F_4$ (a) and its polyhedral showing the octagonal tunnels along the *c* axis (b).

adjacent tunnels together. Ba3 coordinates with seven O atoms (2.565(13)−2.873(8) Å) and two F atoms (2.962(8) Å) and links to the $B2O_3$ groups to support the Ba1 tunnel walls. In this part of the structure there is little difference between $NaBa_{12}(BO_3)_7F_4$ and its Li counterpart with all Ba sites having exactly the same coordination environments and nearly the same bond lengths as those in the Li compound (Table 2).

Table 2. Selected Bond Distances (Angstoms) and Angles (degrees) for $LiBa_{12}(BO_3)_7F_4$ and $NaBa_{12}(BO_3)_7F_4$

$LiBa_{12}(BO_3)_7F_4$			
Ba1−O1	2.941(7)	Ba3−F × 2	2.962(8)
Ba1−O2	2.9634(8)	Li−O5	1.75(7)
Ba1−O3	2.726(6)	Li−F × 4	2.078(14)
Ba1−O4	2.726(7)	B1−O3	1.40(2)
Ba1−O4	2.846(8)	B1−O4	1.376(10)
Ba1−O4	3.049(8)	B2−O1 × 2	1.379(12)
Ba1−O5 × 0.5	2.9085(9)	B3−O5	1.35(4)
Ba1−O6 × 0.25	2.52(2)	B3−O6 × 2	1.37(2)
Ba1−O6 × 0.25	2.74(2)	O5−Li−F	99(2)
Ba1−O6 × 0.25	2.75(2)	F−Li−F	88.5(6)
Ba1−F	2.823(5)	O4−B1−O4	121.9(13)
Ba1−F	2.916(5)	O4−B1−O3	119.1(6)
Ba2−O1 × 4	2.836(6)	O1−B2−O1	121(2)
Ba2−O3 × 2	2.618(9)	O1−B2−O2	119.6(8)
Ba3−O1 × 2	2.688(8)	O5−B3−O6	119.3(12)
Ba3−O2	2.565(13)	O6−B3−O6	121(2)
Ba3−O4 × 4	2.873(8)		
$NaBa_{12}(BO_3)_7F_4$			
Ba1−O1	2.946(5)	Ba3−F × 2	2.827(5)
Ba1−O2	2.9641(6)	Na−O5	2.23(2)
Ba1−O3	2.711(4)	Na−F × 4	2.212(5)
Ba1−O4	2.739(6)	B1−O3	1.390(13)
Ba1−O4	2.871(6)	B1−O4	1.393(8)
Ba1−O4	3.019(6)	B2−O1 × 2	1.380(9)
Ba1−O5 × 0.5	2.956(2)	B3−O5	1.52(2)
Ba1−O6 × 0.25	2.53(2)	B3−O6 × 2	1.31(2)
Ba1−O6 × 0.25	2.87(3)	F−Na−F	90
Ba1−F	2.834(4)	F−Na−O5	90
Ba1−F	2.961(4)	O3−B1−O4	119.5(5)
Ba2−O1 × 4	2.831(4)	O4−B1−O4	121.0(10)
Ba2−O3 × 2	2.616(7)	O2−B2−O1	120.6(5)
Ba3−O1 × 2	2.716(6)	O1−B2−O1	118.8(11)
Ba3−O2	2.582(9)	O6−B3−O6	134(2)
Ba3−O4 × 4	2.909(6)	O6−B3−O5	113.0(11)

dx.doi.org/10.1021/ic4025525 | *Inorg. Chem.* 2014, 53, 2501−2505

Within the octagonal tunnels (Figure 1b), Li/NaF_4O square pyramids and $B3O_3$ groups join together by sharing the O5 atom, forming Li/NaF_4–BO_3 units (Figure 2). The main

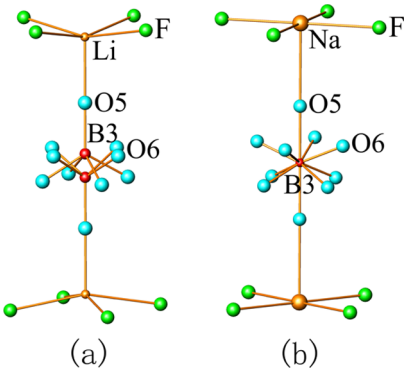

Figure 2. Coordination of LiF_4–BO_3 (a) and NaF_4–BO_3 (b) in the tunnels, showing all possible Li/Na/B3 configurations and all possible oxygen sites in both compounds.

difference between the structures of the title compounds is that the Li atoms and B atoms of the $B3O_3$ groups in the tunnels are disordered and occupy split positions (Figure 2a and Figure S4, Supporting Information), whereas Na and B3 fully occupy the special positions of (0, 0, 0) and (0, 0, 0.25), respectively (Figure 2b). In the NaF_4O pyramid the bond distances of Na–F (2.212(5) Å) and Na–O (2.234(19) Å) are noticeably longer than that of Li–F (2.078(14) Å) and Li–O (1.75(7) Å), which can be attributed to the increasing atom radius of the alkali metal cation. The splitting of B and Li positions in the structure of Li compounds actually was governed by the sum of the ideal bond lengths of Li–O (around 1.99 Å)[25] and B–O (around 1.38 Å),[26] which is far from the fit of the *c* lattice (*c*/4 = 3.748 Å), whereas that of the Na compound with a Na–O bond length of 2.39 Å is much closer (3.77 Å), which is ideal to fit the space (3.755 Å).

Powder second-harmonic generation of the Nd:YAG laser shows that the Li-containing compound generates very weak green light, which means that the $B3O_3$ groups in the tunnels may be partially ordered and point to the same direction, leading to a polar structure. However, due to twining of the crystal and the quality of the diffraction data, refinements on the polar space groups did not give improved results.

A hexagonal Ca tunnel parallel to the *c* axis is also a main structure feature of fluorapatite $Ca_5(PO_4)_3F$, which can host anions like OH^-, Cl^-, CO_3^{2-}, etc. When the F site is replaced by CO_3, statistical disorder and partial ordering of CO_3 were also reported.[27] Other borates with fluorapatite-type structures are $Ca_5(BO_3)_3F$, $Eu_5(BO_3)_3F$, $RbSr_4(BO_3)_3$, and $RCa_4(BO_3)_3O$ (*R* = Y or Gd).[28−30] Recently, in the process of exploring the BaB_2O_4–BaF_2–BaO phase diagram a new borate fluoride salt $Ba_7(BO_3)_{4-2x}F_{2+3x}$ with hexagonal tunnels was discovered. It is isomorphic to $Ba_{4-x}Sr_{3+x}(BO_3)_{4-y}F_{2+3y}$, and both of the compounds belong to the hexagonal system. One main difference of the title compounds from the above-listed compounds concentrates on the tunnels formed: much bigger octagonal tunnels (with radius of 5.89 Å) are found in the former which can host bigger entities, whereas hexagonal tunnels are much smaller (with radii around 5.10 Å) in all structures of the latter compounds.

The grown $LiBa_{12}(BO_3)_7F_4$ crystal shows a purple color (Figure 3, inset), though there is no obvious electron transition

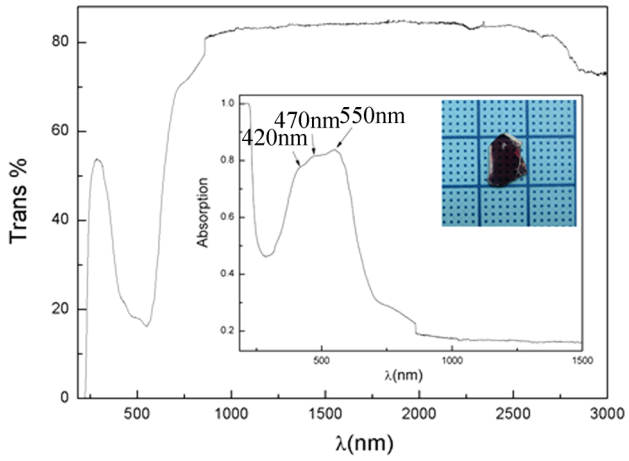

Figure 3. Transmittance spectrum of $LiBa_{12}(BO_3)_7F_4$; (insets) absorption peaks and crystal used in the transmittance spectrum measurement.

that can cause visible light absorption. The transmittance spectrum shows that the crystal is transparent (higher than 80%) in the infrared range, and the UV transparent cutoff edge is 220 nm (Figure 3). One significant feature in the transmittance spectrum is the existence of a strong absorption band ranging from 300 to 700 nm. In order to rule out color center absorption, we irradiated the crystal by a 355 nm laser and annealed the crystal at high temperatures in air, in which the purple color sustains all treatments. This evidence indicates that the broad absorption is extrinsic and probably due to the impurity of the crystal.

The ICP-OES tests show that besides elemental contents of Ba:Li:B = 12:1.06:6.36 in the Li compound and Ba:Na:B = 12:1.3:7.7 in the Na analogue, which is in good accordance with the stoichiometric ratio of $LiBa_{12}(BO_3)_7F_4$ and Na-$Ba_{12}(BO_3)_7F_4$, 0.0033 mol of Cr per mole of $LiBa_{12}(BO_3)_7F_4$ have been detected in $LiBa_{12}(BO_3)_7F$. The Cr element was not found in the Na-containing sample which is colorless, and other common transition metal elements were not detected. Since it is well known that Cr^{3+}-doped crystals can show colors of red or purple (e.g., Ruby = $Cr:Al_2O_3$), it can be concluded that the d–d electron transition of Cr^{3+}ion ($(t_2^3)\ ^4A_2 \rightarrow (t_2^2e)\ ^4T_2, ^4T_1$) is responsible for the absorption bands at 420, 470, and 550 nm (Figure 3. Inset) .[31] Cr^{3+} is likely to substitute the Li ion. Considering its atomic radius,[25] it may perfectly sit at the ordered (0, 0, 0) site. To maintain charge balance that would result in two other lithium vacancies elsewhere in the structure, but since Cr^{3+} is present at such low concentrations it is unlikely to affect the crystallography. To find the source of Cr^{3+}, we have performed the ICP tests for the raw materials of BaF_2 and $BaCO_3$, but Cr^{3+} was not detectable. The crucible used in the experiment was made from Pt with 99.95% or higher purity. Therefore, we speculate that Cr^{3+} is from the vaporized fluoride corrupting the heating wire and transporting Cr back into the melt. For the Na compound in the latter repeating experiments we also got the Na analog with a light pink color (Figure S5, Supporting Information), which may indicate the same problem also exists in a lesser extent, probably due to a higher boiling point of NaF.

Li-ion-containing electrode materials usually have channels in their structures (e.g., $LiFePO_4$), which provide Li ion passage ways.[32] In the title compound Li lies in the tunnels and may have large mobility along the *c* direction. A Cole–Cole plot of

dx.doi.org/10.1021/ic4025525 | *Inorg. Chem.* 2014, 53, 2501−2505

the impedance of a $LiBa_{12}(BO_3)_7F_4$ single crystal along the *c* axis is shown in Figure 4. At 300 °C the conductivity of

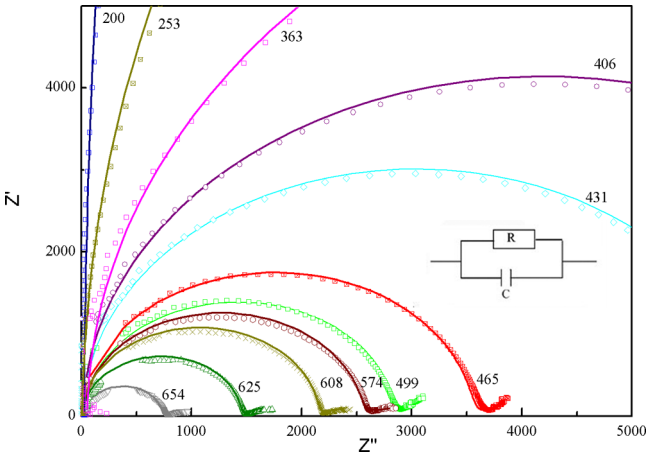

Figure 4. Cole–Cole plot of the $LiBa_{12}(BO_3)_7F_4$ single crystal at different temperatures; numbers in the figure are the corresponding temperatures (°C).

$LiBa_{12}(BO_3)_7F_4$ is 1×10^{-6} S·cm^{-1}, and when the temperature is elevated to above 500 °C, the conductivity is larger than 10^{-5} S·cm^{-1}. The nearly linear dependence of lg(σ) vs 1000/*T* (Figure 5) indicates that ion diffusion in the $LiBa_{12}(BO_3)_7F_4$

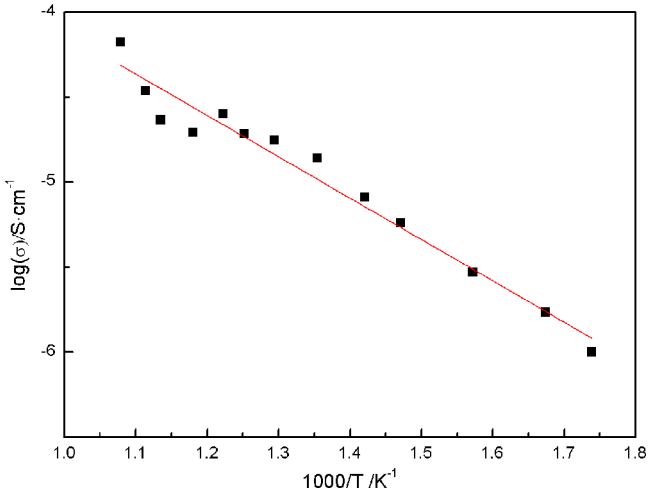

Figure 5. Temperature dependence of bulk ionic conductivities of $LiBa_{12}(BO_3)_7F_4$.

crystal follows the Arrhenius relation. The activation energy (E_a) for Li diffusion along the *c* axis can be extracted as 0.54 ± 0.026 eV. Both the conductivity and the activation energy are at the same level of the electrode material $LiFePO_4$ when measured in single-crystal form, e.g., in $LiFePO_4$ the conductivity (525 K) and the activation energy along the *b* axis, which has the largest conductivity among the axes, are 4.76×10^{-6} S·cm^{-1} and 0.54 ± 0.048 eV.[33] In addition, TG-DSC measurements demonstrate that the $LiBa_{12}(BO_3)_7F_4$ crystal is stable below 900 °C (Figure S2, Supporting Information). At elevated temperature this lithium borate fluoride can be regarded as a solid electrolyte according to the classification suggested by Tuller and Moon[34] and may find potential applications.[35]

CONCLUSIONS

Two new borate fluoride crystals $LiBa_{12}(BO_3)_7F_4$ and $NaBa_{12}(BO_3)_7F_4$ were obtained by spontaneous crystallization. The two compounds are isostructural with *I*4/*mcm* space group. Octagonal tunnels are found in the structures of the two compounds which resemble the hexagonal tunnels in the fluorapatite structures. MF_4–BO_3 (M = Li and Na) units were found to occupy the tunnels. $LiBa_{12}(BO_3)_7F_4$ crystals with sizes up to 20 × 30 × 30 mm^3 have been grown by the TSSG method. The purple color of the grown $LiBa_{12}(BO_3)_7F_4$ crystal was found to originate from the tiny amount of Cr^{3+} impurity. Li ions in the tunnels were found possessing high mobility with conductivity larger than 10^{-5} S·cm^{-1} above 500 °C, and the activation energy is 0.54 ± 0.026 eV. The $LiBa_{12}(BO_3)_7F_4$ crystal is stable up to 900 °C and could potentially find application as a high-temperature Li-ion electrolyte.

ASSOCIATED CONTENT

Supporting Information

Electronic files of the crystal structure data (CIF), and listings of tables of atomic coordinates, equivalent isotropic temperature factors, BVS, XRD patterns, TG-DSC curve, and Raman spectroscopy. This material is available free of charge via the Internet at http://pubs.acs.org.

AUTHOR INFORMATION

Corresponding Author

*E-mail: rkli@mail.ipc.ac.cn.

Notes

The authors declare no competing financial interest.

ACKNOWLEDGMENTS

This work was supported by a grant from the National Science Foundation of China (Nos. 90922036 and 51032004/E0201).

REFERENCES

(1) (a) Rowsell, J. L. C.; Taylor, N. J.; Nazar, L. F. *J. Am. Chem. Soc.* **2002**, *124*, 6522–6523. (b) Janssen, Y.; Middlemiss, D. S.; Bo, S.; Grey, C. P.; Khalifah, P. G. *J. Am. Chem. Soc.* **2012**, *134*, 12516–12527.

(2) (a) Yang, T.; Bartoszewicz, A.; Ju, J.; Sun, J.; Liu, Z.; Zou, X.; Wang, Y.; Li, G.; Liao, F.; Martín-Matute, B.; Lin, J. *Angew. Chem., Int. Ed.* **2011**, *50*, 12555–12558. (b) Wang, S.; Alekseev, E. V.; Ling, J.; Liu, G.; Depmeier, W.; Albrecht-Schmitt, T. E. *Chem. Mater.* **2010**, *22*, 2155–2163.

(3) (a) Zhang, W.; Cheng, W.; Zhang, H.; Geng, L.; Lin, C.; He, Z. *J. Am. Chem. Soc.* **2010**, *132*, 1508–1509. (b) Wang, S.; Ye, N. *J. Am. Chem. Soc.* **2011**, *133*, 11458–11461. (c) Huang, H.; Yao, J.; Lin, Z.; Wang, X.; He, R.; Yao, W.; Zhai, N.; Chen, C. *Angew. Chem., Int. Ed.* **2011**, *123*, 9307–9310.

(4) (a) Jin, S.; Cai, G.; Wang, W.; He, M.; Wang, S.; Chen, X. *Angew. Chem. Int.Ed.* **2010**, *49*, 4967–4970. (b) Wu, Y.; Yao, J. Y.; Zhang, J. X.; Fu, P. Z.; Wu, Y. C. *Acta Crystallogr.* **2010**, *E66*, i45.

(5) Touboul, M.; Penin, N.; Nowogrocki, G. *Solid State Sci.* **2003**, *5*, 1327–1342.

(6) Chen, C.; Wang, Y.; Xia, Y.; Wu, B.; Tang, D.; Wu, K.; Zeng, W.; Yu, L.; Mei, L. *J. Appl. Phys.* **1995**, *77*, 2268–2272.

(7) Keszler, D. A.; Akella, A.; Schaffers, K. I.; Alekel, T. *Mater. Res. Soc. Symp. Proc.* **1994**, *329*, 15–22.

(8) Li, R. K.; Chen, P. *Inorg. Chem.* **2010**, *49*, 1561–1565.

(9) (a) Park, H.; Barbier, J. *J. Solid State Chem.* **2000**, *155*, 354–358. (b) Hu, Z. G.; Maramatsu, K.; Kanehisa, N.; Yoshimura, M.; Mori, Y.; Sasaki, T.; Kai, Y. *Z. Kristallogr.-New Cryst. Struct.* **2003**, *218*, 1–2. (c) Hu, Z.; Yue, Y.; Chen, X.; Yao, J.; Wang, J.; Lin, Z. *Solid State Sci.* **2011**, *13*, 875–878.

(10) (a) Brovkin, A. A.; Nikishova, L. V. *Sov. Phys. Crystallogr.* **1975**, *20*, 252−254. (b) Lei, S.; Huang, Q.; Zheng, Y.; Jiang, A.; Chen, C. *Acta Crystallogr.* **1989**, *C45*, 1861−1863.
(11) Mcmillen, C. D.; Stritzinger, J. T.; Kolis, J. W. *Inorg. Chem.* **2012**, *51*, 3953−3955.
(12) Mei, L. F.; Wang, Y. B.; Chen, C. T. *Mater. Res. Bull.* **1994**, *29*, 81−87.
(13) (a) Kokh, A. E.; Kononova, N. G.; Bekker, T. B.; Fedorov, P. P.; Nigmatulina, E. A.; Ivanova, A. G. *Crystallogr. Rep.* **2009**, *54*, 146−151. (b) Bekker, T. B; Kokh, A. E.; Kononova, N. G.; Fedorov, P. P.; Kuznetsov, S. V. *Cryst. Growth Des.* **2009**, *9*, 4060−4063. (c) Bekker, T. B.; Kononova, N. G.; Kokh, A. E.; Kuznetsov, S. V.; Fedorov, P. P. *Crystallogr. Rep.* **2010**, *55*, 877−881.
(14) Rashchenko, S. V.; Bekker, T. B.; Bakakin, V. V.; Seryotkin, Yu. V.; Shevchenko, V. S.; Kokh, A. E.; Stonoga, S. Yu. *Cryst. Growth Des.* **2012**, *12*, 2955−2960.
(15) Alekel, T.; Keszler, D. A. *J. Solid State Chem.* **1993**, *106*, 310−316.
(16) Bekker, T. B.; Rashchenko, S. V.; Bakakin, V. V.; Seryotkin, Yu. V.; Fedorov, P. P.; Kokh, A. E.; Stonoga, S. Yu. *CrystEngComm.* **2012**, *14*, 6910−6915.
(17) Keszler, D. A.; Akella, A.; Schaffers, K. I.; Alekel, T. *Mater. Res. Soc. Symp. Proc.* **1994**, *329*, 15−22.
(18) Etheredge, K. M. S.; Hwu, S. J. *Inorg. Chem.* **1995**, *34*, 3123−3125.
(19) Huang, Q.; Hwu, S. J. *Inorg. Chem.* **2003**, *42*, 655−657.
(20) Li, R. K.; Yu, Y. *Inorg. Chem.* **2006**, *45*, 6840−6843.
(21) Liao, C. H.; Chang, P. C.; Kao, H. M.; Lii, K. H. *Inorg. Chem.* **2005**, *44*, 9335−9339.
(22) Yu, H.; Wu, H.; Pan, S.; Wang, Y.; Yang, Z.; Su, X. *Inorg. Chem.* **2013**, *52*, 5359−5365.
(23) *Crystalclear*; Rigaku Corp.: Tokyo, Japan, 2008.
(24) Sheldrick, G. M. *Acta Crystallogr.* **2008**, *A64*, 112−122.
(25) Shannon, R. D. *Acta Crystallogr.* **1976**, *A32*, 751−767.
(26) Wells, A. F. *Structure of Chemistry*; Oxford University Press: Oxford, 1984.
(27) (a) Suetsugu, Y.; Takahashi, Y.; Okamura, F. P.; Tanaka, J. *J. Solid State Chem.* **2000**, *155*, 292−297. (b) Tonegawa, T.; Ikoma, T.; Yoshioka, T.; Hanagata, N.; Tanaka, J. *J. Mater. Sci.* **2010**, *45*, 2419−2426.
(28) Kazmierczak, K.; Höppe, H. A. *Eur. J. Inorg. Chem.* **2010**, *18*, 2678−2681.
(29) Xia, M. J.; Li, R. K. *J. Solid State Chem.* **2013**, *197*, 366−369.
(30) Norrestam, R.; Nygren, M.; Bovin, J. O. *Chem. Mater.* **1992**, *4*, 737−743.
(31) Fairbank, W. M., Jr.; Klauminzer, G. K.; Schawlow, A. L. *Phys. Rev. B* **1975**, *11*, 60−76.
(32) Yang, J.; Tse, J. S. *J. Phys. Chem. A* **2011**, *115*, 13045−13049.
(33) Li, J.; Yao, W.; Martin, S.; Vaknin, D. *Solid State Ionics* **2008**, *179*, 2016−2019.
(34) Tuller, H. L.; Moon, P. K. *Mater. Sci. Eng., B* **1988**, *1*, 171−191.
(35) Robertson, A. D.; West, A. R.; Ritchie, A. G. *Solid State Ionics* **1997**, *104*, 1−11.

dx.doi.org/10.1021/ic4025525 | *Inorg. Chem.* 2014, 53, 2501−2505